

1 **A spatial skew-*t* model for threshold exceedances**

2 July 22, 2015

3 **1 Introduction**

4 In many climatological applications, researchers are interested in learning about the average behavior of
5 different climate variables (e.g. ozone, temperature, rainfall). Our study is motivated by an air pollution
6 application where the focus is not on the average behavior, but instead the behavior over a fixed threshold
7 determined by government regulation. More specifically, we consider consider the case of compliance for
8 ozone. A site is said to be in compliance if the fourth highest daily maximum 8-hour concentration averaged
9 over 3 years does not exceed 75 parts per billion (ppb).

10 Traditional geostatistical modeling is based upon the assumption that observations come from a Gaussian
11 process, a process that is fully defined by its mean and covariance functions. In the limit of the Gaussian
12 distribution, all observations are independent regardless of the strength of the correlation in the bulk of the
13 data. Furthermore, the Gaussian distribution is light-tailed and symmetric. Therefore, it is inappropriate to
14 use standard geostatistical methods when trying to describe dependence in the tails of the distribution.

15 Threshold modeling is popular in the field of extreme value statistics where extreme events are naturally
16 defined in terms of exceedances over a high threshold. Davison and Smith (1990) considered modeling
17 threshold exceedances of univariate time series by the generalized Pareto distribution. Bivariate threshold
18 models for extreme value distributions were considered by Ledford and Tawn (1996) who introduced a
19 censored approach that provides a way to deal with different types of exceedances of a bivariate threshold in
20 terms of only one or both components. These threshold models were extended to spatial models for extremes
21 by Wadsworth and Tawn (2012) and Thibaud et al. (2013) who fit various models to spatial extremes using a
22 censored pairwise likelihood (Padoan et al., 2010) based on the approach of Ledford and Tawn (1996). Huser

23 and Davison (2014) further extended this to spate-time modeling. Engelke et al. (2014), Wadsworth and
24 Tawn (2014), and Thibaud and Opitz (2013) introduced more efficient inference for threshold exceedances
25 of extremal spatial processes with full likelihood methods. The previous approaches to threshold modeling
26 are motivated by extreme value theory and assume the threshold is high enough to assume extremal models
27 are valid for the data, and for extrapolation beyond the range of observed values. Moreover, these approaches
28 are computationally intensive and limited to rather small datasets. Our application with ozone data does not
29 fit into this framework because we do not focus on exceedances of a very high threshold, but on exceedances
30 of a fixed threshold.

31 Instead, we propose a new spatiotemporal threshold exceedance model based on the skew-*t* process
32 (Padoan, 2011). Our model is a threshold exceedance model for the multivariate skew-*t* distribution that
33 uses imputation for values below a fixed threshold. We use a skew-*t* distribution because of its flexibility to
34 model asymmetry and heavy-tailed data with the aim of predicting the probability of exceeding a high fixed
35 threshold at an unobserved location.

36 In a spatial setting, the multivariate skew-*t* distribution demonstrates asymptotic dependence between
37 observations at all sites regardless of the distance between the sites. In order to address this concern, we
38 introduce a random spatial partition similar to the method used by Kim et al. (2005) for non-stationary
39 Gaussian data. This partition alleviates the asymptotic spatial dependence present in the skew-*t* distribution
40 for sites that are far apart. Finally, our model allows for inference and predictions using the full likelihood
41 with computing on the order of Gaussian models for large space-time datasets.

42 The paper is organized as follows. Section 2 is a brief review of the spatial skew-*t* process. In Section
43 3.3, we build upon the traditional skew-*t* by incorporating censoring to focus on tails, partitioning to remove
44 long-range asymptotic dependence, and extending the model to space-time data. The computing is described
45 in Section 4.1. In Section 5, we present a simulation study that examines the predictive capabilities of this

46 model compared with a naïve Gaussian method. We then compare our method to Gaussian and max-stable
 47 methods with a data analysis of ozone measurements from throughout the US in section 6. The final section
 48 provides brief discussion and direction for future research.

49 **2 Spatial skew processes**

50 Many types of data demonstrate some level of skewness and therefore should be modeled with distributions
 51 that allow for asymmetry. The skew-elliptical family of distributions provides models that are mathemati-
 52 cally tractable while introducing a slant parameter to account for asymmetric data (Genton, 2004). A brief
 53 review of the additive process by which a skew- t process is created is given here.

54 **2.1 Skew- t process**

55 Let $Y(\mathbf{s})$ be the observation at spatial location $\mathbf{s} = (s_1, s_2)$ in a spatial domain of interest $\mathcal{D} \in \mathcal{R}^2$. The
 56 spatial skew- t process can be written

$$Y(\mathbf{s}) = \mathbf{X}(\mathbf{s})^T \boldsymbol{\beta} + \lambda \sigma |z| + \sigma v(\mathbf{s}) \quad (1)$$

57 where $\mathbf{X}(\mathbf{s})$ is a set of spatial covariates at site \mathbf{s} , $\boldsymbol{\beta}$ is the vector of regression parameters, $\lambda \in \mathcal{R}$ is a
 58 parameter controlling skew, $z \sim N(0, 1)$, $\sigma^2 \sim \text{IG}(a, b)$ is an inverse gamma random variable, and $v(\mathbf{s})$ is
 59 a spatial Gaussian process with mean zero, variance one, and a positive definite correlation function.

60 For a finite collection of locations $\mathbf{s}_1, \dots, \mathbf{s}_n$, denote the vector of observations $\mathbf{Y} = [Y(\mathbf{s}_1), \dots, Y(\mathbf{s}_n)]^T$.

61 After marginalizing over both z and σ ,

$$\mathbf{Y} \sim \text{ST}_n(\mathbf{X}\boldsymbol{\beta}, \boldsymbol{\Omega}, \boldsymbol{\alpha}, 2a), \quad (2)$$

62 that is, \mathbf{Y} follows an n -dimensional skew- t distribution with location $\mathbf{X}\boldsymbol{\beta}$, correlation matrix $\boldsymbol{\Omega}$, slant parameters $\boldsymbol{\alpha}$ and degrees of freedom $2a$, where $\mathbf{X} = [\mathbf{X}(\mathbf{s}_1)^T, \dots, \mathbf{X}(\mathbf{s}_n)^T]$, $\boldsymbol{\Omega} = \boldsymbol{\omega}\bar{\boldsymbol{\Omega}}\boldsymbol{\omega}$, $\boldsymbol{\omega} = \text{diag}\left(\frac{1}{\sqrt{ab}}, \dots, \frac{1}{\sqrt{ab}}\right)$,
 63 $\bar{\boldsymbol{\Omega}} = (\boldsymbol{\Sigma} + \lambda^2 \mathbf{1}\mathbf{1}^T)$, $\boldsymbol{\Sigma}$ is the positive definite correlation matrix of $[v(\mathbf{s}_1), \dots, v(\mathbf{s}_n)]$, $\boldsymbol{\alpha} = \lambda(1 + \lambda^2 \mathbf{1}^T \boldsymbol{\Sigma}^{-1} \mathbf{1})^{-1/2} \mathbf{1}^T \boldsymbol{\Sigma}^{-1}$
 64 is a vector of slant parameters. Although any positive definite correlation function could be used, we choose
 65 to use the stationary isotropic Matérn correlation with

$$\text{cor}[v(\mathbf{s}), v(\mathbf{t})] = \gamma I(\mathbf{s} = \mathbf{t}) + (1 - \gamma) \frac{1}{\Gamma(\nu) 2^{\nu-1}} \left(\sqrt{2\nu} \frac{h}{\rho} \right)^\nu K_\nu \left(\sqrt{2\nu} \frac{h}{\rho} \right) \quad (3)$$

67 where ρ is the spatial range, ν is the smoothness, γ is the proportion of variance accounted for by the
 68 spatial variation, K_ν is a modified Bessel function of the second kind, and $h = \|\mathbf{s} - \mathbf{t}\|$. This process is
 69 desirable because of its flexible tail that is controlled by the skewness parameter λ and degrees of freedom
 70 $2a$. Furthermore, the marginal distributions at each location also follow a univariate skew- t distribution
 71 (Azzalini and Capitanio, 2014).

72 2.2 Extremal dependence

73 Our interest lies in spatial dependence in the tail of the skew- t process. One measure of extremal dependence
 74 is the χ statistic (Coles et al., 1999). For a stationary and isotropic spatial process, the χ statistic for locations
 75 \mathbf{s} and \mathbf{t} separated by distance $h = \|\mathbf{s} - \mathbf{t}\|$ with identical marginal distributions is

$$\chi(h) = \lim_{c \rightarrow c^*} \Pr[Y(\mathbf{s}) > c | Y(\mathbf{t}) > c] \quad (4)$$

76 where c^* is the upper limit of the support of Y . If $\chi(h) = 0$, then observations are asymptotically indepen-
 77 dent at distance h . For Gaussian processes, $\chi(h) = 0$ regardless of the distance h , so they are not suitable for
 78 modeling asymptotically dependent extremes. Unlike the Gaussian process, the skew- t process is asymptot-

79 ically dependent (the explicit expression for $\chi(h)$ is given in Appendix A.4). However, one problem with
 80 the spatial skew- t process is that $\lim_{h \rightarrow \infty} \chi(h) > 0$. This occurs because all observations, both near and
 81 far, share the same z and σ terms. Therefore, this long-range dependence feature of the skew- t process is
 82 not ideal for spatial analysis of large geographic regions where we expect only local spatial dependence.

83 **3 Spatiotemporal skew- t model for extremes**

84 In this section, we propose extensions to the skew- t process to model spatial extremes over a large geo-
 85 graphic region by introducing censoring to focus on tail behavior and a random partition to remove long-
 86 range asymptotic dependence. For notational convenience, we introduce the model for a single replication,
 87 and then extend this model to the spatiotemporal setting in Section 3.3.

88 **3.1 Censoring to focus on the tails**

89 Because one of our goals is to model the dependence of the distribution in the tails of the data, we choose to
 90 censor values below threshold. Let

$$\tilde{Y}(\mathbf{s}) = \begin{cases} Y(\mathbf{s}) & \delta(\mathbf{s}) = 1 \\ T & \delta(\mathbf{s}) = 0 \end{cases} \quad (5)$$

91 be the censored observation at site \mathbf{s} where $Y(\mathbf{s})$ is the uncensored observation, $\delta(\mathbf{s}) = I[Y(\mathbf{s}) > T]$, and T
 92 is a pre-specified threshold value. Then, assuming the uncensored data $Y(\mathbf{s})$ are observations from a skew- t
 93 process, we update values censored below the threshold using standard Bayesian missing data methods as
 94 described in Section 4.1.

95 **3.2 Partitioning to remove long-range asymptotic dependence**

96 The motivation for the partition is that for a large spatial domain, it may not be reasonable to assume sites
 97 that are far apart demonstrate asymptotic dependence. Modeling different levels of asymptotic dependence
 98 was discussed by Wadsworth and Tawn (2012) with a hybrid spatial dependence model. Huser and Davison
 99 (2014) also allow for asymptotic dependence across both space and time with a partition structure repre-
 100 sented by random discs moving across the space for a random duration with a random velocity and random
 101 radius. We handle the problem of long-range asymptotic dependence with a random partition. As dis-
 102 cussed in Section 2, the source of long-range dependence is the shared z and σ . Therefore, to alleviate this
 103 dependence, we allow z and σ to vary by site. The model becomes

$$Y(\mathbf{s}) = \mathbf{X}(\mathbf{s})^T \boldsymbol{\beta} + \lambda \sigma(\mathbf{s})|z(\mathbf{s})| + \sigma(\mathbf{s})v(\mathbf{s}). \quad (6)$$

104 Let $\mathbf{w} = (w_1, w_2)$ be the location of a spatial knot. To model spatial variation, consider a set of spatial knots
 105 $\mathbf{w}_1, \dots, \mathbf{w}_K$ from a homogeneous Poisson process with intensity μ over spatial domain $\mathcal{D} \in \mathbb{R}^2$. The knots
 106 define a random partition of \mathcal{D} by subregions P_1, \dots, P_K defined as

$$P_k = \{\mathbf{s} : k = \arg \min_\ell \|\mathbf{s} - \mathbf{w}_\ell\|\}. \quad (7)$$

107 All $z(\mathbf{s})$ and $\sigma(\mathbf{s})$ for sites in subregion k are assigned common values

$$z(\mathbf{s}) = z_k \quad \text{and} \quad \sigma(\mathbf{s}) = \sigma_k \quad (8)$$

108 and the z_k and σ_k^2 are distributed as $z_k \stackrel{iid}{\sim} N(0, 1)$ and $\sigma^2 \stackrel{iid}{\sim} \text{IG}(a, b)$ where IG is the distribution function
 109 of an inverse gamma random variable. So, within each partition, $Y(\mathbf{s})$ follows the spatial skew- t process

110 defined in Section 2. Across partitions, the $Y(\mathbf{s})$ remain correlated via the correlation function for $v(\mathbf{s})$
111 because $v(\mathbf{s})$ spans all partitions.

112 When incorporating the random partition, conditional on knots $\mathbf{w}_1, \dots, \mathbf{w}_K$, the χ statistic for two sites
113 \mathbf{s} and \mathbf{t} in partitions k_s and k_t respectively is

$$\begin{aligned}\chi(h) &= I(k_s = k_t)\chi_{\text{skew-}t}(h) + I(k_s \neq k_t)\chi_{\text{Gaus}}(h) \\ &= I(k_s = k_t)\chi_{\text{skew-}t}(h)\end{aligned}\tag{9}$$

114 where $I(\cdot)$ is an indicator function, $\chi_{\text{skew-}t}(h)$ is the χ statistic for a skew- t process given in (29), $\chi_{\text{Gaus}}(h)$
115 is the χ statistic for a Gaussian process, and $h = \|\mathbf{s} - \mathbf{t}\|$. Therefore, sites in different subregions are
116 asymptotically independent because $\chi_{\text{Gaus}}(h) = 0$ for all h . Marginally, over the knots $\mathbf{w}_1, \dots, \mathbf{w}_K$, $\chi(h) =$
117 $\pi(h)\chi_{\text{skew-}t}(h)$, where $\pi(h) = \Pr(k_s = k_t)$ is the probability that two sites separated by distance h are in
118 the same partition. So, to show that $\lim_{h \rightarrow \infty} \chi(h) = 0$, we need only know that $\lim_{h \rightarrow \infty} \pi(h) = 0$. A proof
119 of this is given in Appendix A.3.

120 In Figure 1, we give $\chi(h)$ for $K = 1, 3, 5, 10$ partitions for a skew- t distribution with $\alpha = 10$, and
121 3 degrees of freedom. To estimate $\pi(h)$, we generate 500 sites uniformly over the unit-square. We then
122 randomly generate 400 different sets of partitions using $K = 3, 5$, and 10. For each set of knots, we
123 take $\pi(h)$ to be the proportion of sites in the same partition that are separated by distance h . This plot
124 demonstrates how partitioning helps to reduce extremal dependence as h increases.

125 3.3 Extension to space-time data

126 When using daily measurements, the assumption of temporal independence is often inappropriate. In this
127 section, we extend (6) to the spatiotemporal setting. There are several places where temporal dependence
128 could be incorporated in the model, including the residuals $v_t(\mathbf{s})$. However, we choose to allow for temporal

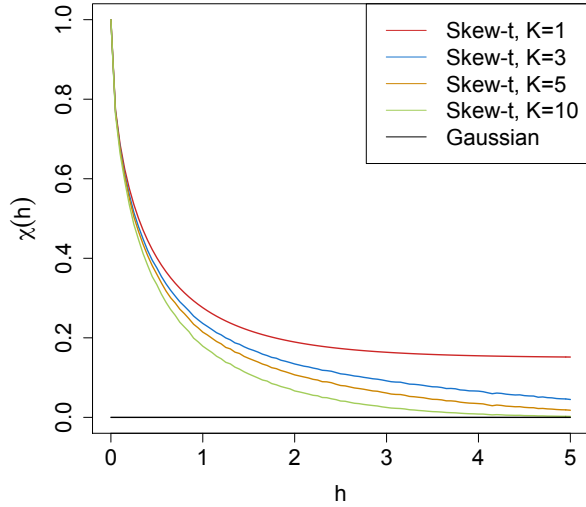


Figure 1: $\chi(h)$ for $K = 1, 3, 5$, and 10 knots as a function of distance.

129 dependence in the \mathbf{w} , z , and σ terms because these terms dictate the tail behavior which is our primary focus.

130 Let

$$Y_t(\mathbf{s}) = \mathbf{X}_t(\mathbf{s})^T \boldsymbol{\beta} + \lambda \sigma_t(\mathbf{s}) |z_t(\mathbf{s})| + \sigma_t(\mathbf{s}) v_t(\mathbf{s}), \quad (10)$$

131 where $t \in \{1, \dots, T\}$ denotes the day of each observation. Let $\mathbf{w}_{tk} = (w_{tk1}, w_{tk2})$ be a spatial knot on day

132 t , and let w_{t1}, \dots, w_{tK} be a collection of spatial knots on day t . As in Section 3.2, these knots define a daily

133 partition P_{t1}, \dots, P_{tK} , and for $\mathbf{s} \in P_{tk}$,

$$z_t(\mathbf{s}) = z_{tk} \quad \text{and} \quad \sigma_t(\mathbf{s}) = \sigma_{tk}. \quad (11)$$

134 We allow the partition structure to vary from day to day in order to account for sharp spikes in ozone that

135 may not be present every day (e.g. a forest fire).

136 We use an AR(1) time series model for w_{tk} , z_{tk} , and σ_{tk} . The time series model must be specified after

137 a transformation to preserve the skew- t process at each time point. For each time-varying parameter, we
 138 transform to obtain a standard normal marginal distribution, place a Gaussian prior with autocorrelation on
 139 the transformed parameter, and then transform back to obtain the marginal distribution required to preserve
 140 the skew- t process. We first transform the spatial knots from \mathcal{D} to \mathcal{R}^2 as follows. Let

$$w_{tki}^* = \Phi^{-1} \left[\frac{w_{tki} - \min(\mathbf{s}_i)}{\max(\mathbf{s}_i) - \min(\mathbf{s}_i)} \right], \quad i = 1, 2 \quad (12)$$

141 where Φ is a univariate standard normal density function, and $\mathbf{s}_i = [s_{1i}, \dots, s_{ni}]$. Then the transformed
 142 knots $\mathbf{w}_{tk}^* \in \mathcal{R}^2$. We use a copula on $\sigma_t^2(\mathbf{s})$ to ensure that the marginal distributions of $\sigma_t^2(\mathbf{s})$ are inverse
 143 gamma. Let

$$\sigma_t^{2*}(\mathbf{s}) = \Phi^{-1} \{ \text{IG}[\sigma_t^2(\mathbf{s})] \} \quad (13)$$

144 where IG is defined as before. We also use a copula on $z_t(\mathbf{s})$ to ensure that the marginal distributions of
 145 $z_t(\mathbf{s})$ are half-normal. Let

$$z_t^*(\mathbf{s}) = \Phi^{-1} \{ \text{HN}[z_t(\mathbf{s})] \} \quad (14)$$

146 where HN is the distribution function of a half-normal random variable. The AR(1) process for each tail
 147 parameter is $\mathbf{w}_{1k}^* \sim N_w(0, 1)$, $z_{1k}^* \sim N(0, \sigma_{1k}^2)$, $\sigma_{1k}^{2*} \sim N(0, 1)$, and for $t > 1$ the time series is modeled as

$$\mathbf{w}_{tk}^* | \mathbf{w}_{t-1,k}^* \sim N_2 [\phi_w \mathbf{w}_{t-1,k}^*, (1 - \phi_w^2)] \quad (15)$$

$$z_{tk}^* | z_{t-1,k}^* \sim N [\phi_z z_{t-1,k}^*, \sigma_{tk}^2 (1 - \phi_z^2)] \quad (16)$$

$$\sigma_{tk}^{2*} | \sigma_{t-1,k}^{2*} \sim N [\phi_\sigma \sigma_{t-1,k}^{2*}, (1 - \phi_\sigma^2)] \quad (17)$$

148 where $|\phi_w|, |\phi_z|, |\phi_\sigma| < 1$. These are stationary time series models with marginal distributions $\mathbf{w}_k^* \sim N_2(0, 1)$,
149 $z_k^* \sim N(0, \sigma_k^2)$, and $\sigma_k^{2*} \sim N(0, 1)$. After transformation back to the original space, $\mathbf{w}_{tk} \sim \text{Unif}(\mathcal{D})$,
150 $z_{tk} \sim HN(0, \sigma_{tk}^2)$ $\sigma_{tk}^2 \sim \text{IG}(a, b)$. For each day, the model is identical to the spatial-only model in (6)
151 by construction.

152 4 Hierarchical model

153 Conditioned on $z_{tk}(\mathbf{s})$, $\sigma_{tk}^2(\mathbf{s})$, and P_{tk} , the marginal distributions are Gaussian and the joint distribution
154 multivariate Gaussian. However, we do not fix the partitions, they are treated as unknown and updated in the
155 MCMC. We model this with a Bayesian hierarchical model as follows. Let $\mathbf{w}_{t1}, \dots, \mathbf{w}_{tK}$ be a set of daily
156 spatial knots in a spatial domain of interest, \mathcal{D} , and P_{tk} as defined in (7). In practice, we fix K at many

¹⁵⁷ different levels, and assess the impact of fit as described in 5.2. Then

$$Y_t(\mathbf{s}) \mid z_t(\mathbf{s}), \sigma_t^2(\mathbf{s}), P_{tk}, \Theta = \mathbf{X}_t(\mathbf{s})^T \beta + \lambda |z_t(\mathbf{s})| + \sigma_t(\mathbf{s}) v_t(\mathbf{s}) \quad (18)$$

$$z_t(\mathbf{s}) = z_{tk} \text{ if } \mathbf{s} \in P_{tk}$$

$$\sigma_t^2(\mathbf{s}) = \sigma_{tk}^2 \text{ if } \mathbf{s} \in P_{tk}$$

$$\lambda = \lambda_1 \lambda_2$$

$$\lambda_1 = \begin{cases} +1 & \text{w.p. 0.5} \\ -1 & \text{w.p. 0.5} \end{cases}$$

$$\lambda_2^2 \sim IG(a, b)$$

$$v_t(\mathbf{s}) \mid \Theta \sim \text{Matérn}(0, \Sigma)$$

$$z_{tk}^* \mid z_{t-1,k}^*, \sigma_{tk}^2 \sim N(\phi_z z_{t-1,k}^*, \sigma_{tk}^2(1 - \phi_z^2))$$

$$\sigma_{tk}^{2*} \mid \sigma_{t-1,k}^{2*} \sim N(\phi_\sigma \sigma_{t-1,k}^{2*}, (1 - \phi_\sigma^2))$$

$$\mathbf{w}_{tk}^* \mid \mathbf{w}_{t-1,k}^* \sim N_2(\phi_w \mathbf{w}_{t-1,k}^*, (1 - \phi_w^2))$$

¹⁵⁸ where $\Theta = \{\rho, \nu, \gamma, \lambda, \beta\}$, and Σ is a Matérn covariance matrix as described in Section 2.1. We parameterize

¹⁵⁹ $\lambda = \lambda_1 \lambda_2$ to help with convergence in the MCMC.

¹⁶⁰ 4.1 Computation

¹⁶¹ We use Markov chain Monte Carlo methods to explore the posterior. At each MCMC iteration, we first

¹⁶² impute values below the threshold conditional on observations above the threshold. This is feasible for large

¹⁶³ datasets with our model because for a single day, conditional on the model parameters, we only need to draw

¹⁶⁴ from a truncated multivariate normal distribution. We can use Gibbs sampling to update $Y_t(\mathbf{s})$ for censored

¹⁶⁵ observations that are below the threshold T . After conditioning on λ , $z_t(\mathbf{s})$ and non-censored observations,

166 $Y_t(\mathbf{s})$ has truncated normal full conditionals. So we sample $Y_t(\mathbf{s}) \sim N_{(-\infty, T)}(\mathbf{X}_t^T(\mathbf{s})\beta + \lambda|z_t(\mathbf{s})|, \Sigma)$.

167 Then, we update model parameters, Θ , using Metropolis Hastings or Gibbs sampling when appropriate.

168 The final step of the computation is to use Bayesian Kriging to generate a predictive distribution for $Y_t(\mathbf{s}^*)$

169 at prediction location \mathbf{s}^* . This step is similar to the imputation for censored observations except that the full

170 conditionals are no longer truncated at T . See Appendices A.1 and A.2 for details regarding the MCMC.

171 5 Simulation study

172 In this section, we conduct a simulation study to investigate how the number of partitions and the level of

173 thresholding impact the accuracy of predictions made by the model.

174 5.1 Design

175 For all simulation designs, we generate data from the model in Section 3.2 using $n_s = 144$ sites and

176 $n_t = 50$ independent days. The sites are generated Uniform($[0, 10] \times [0, 10]$). We generate data from 5

177 different simulation designs:

178 1. Gaussian marginal, $K = 1$ knot

179 2. Skew- t marginal, $K = 1$ knots

180 3. Skew- t marginal, $K = 5$ knots

181 4. Max-stable

182 5. Transformation below $T = q(0.80)$

183 In the first three designs, the $v_t(\mathbf{s})$ terms are generated using a Matérn covariance with smoothness parameter

184 $\nu = 0.5$ and spatial range $\rho = 1$. For the covariance matrices in designs 1 – 3, the proportion of the variance

185 accounted for by the spatial variation is $\gamma = 0.9$ while the proportion of the variance accounted for by the

186 nugget effect is 0.1. In the first design, $\sigma^2 = 2$ is used for all days which results in a Gaussian distribution.

187 For designs 2 and 3, $\sigma_{tk}^2 \stackrel{iid}{\sim} \text{IG}(3, 8)$ to give a t distribution with 6 degrees of freedom. For design 1, we set
 188 $\lambda = 0$. For designs 2 and 3, $\lambda = 3$ was used as to simulate moderate skewness, and the z_t are generated as
 189 described in (8). In the fourth design, we generate from a spatial max-stable distribution (Reich and Shaby,
 190 2012). In this design, data have marginal distributions that follow a generalized extreme value distribution
 191 with parameters $\mu = 1, \sigma = 1, \xi = 0.2$. In this model, a random effect is used to induce spatial dependence
 192 using 144 spatial knots on a regular lattice in the square $[1, 9] \times [1, 9]$. For this setting, we set $\gamma = 0.5$. In
 193 the final design, we generate \tilde{y} using the setting from design 2, and then transform the data

$$y = \begin{cases} \tilde{y}, & \tilde{y} > T \\ T \exp\{\tilde{y} - T\}, & \tilde{y} \leq T \end{cases} \quad (19)$$

194 where $T = q(0.80)$ is the 80th sample quantile of the data. The final design is included to explore the impor-
 195 tance of using a threshold exceedance model when the distribution for the bulk of the data is misspecified.
 196 In all six designs, the mean $\mathbf{X}^T \boldsymbol{\beta} = 10$ is assumed to be constant across space.

197 $M = 50$ data sets are generated for each design. For each data set we fit the data using five models
 198

1. Gaussian marginal, $K = 1$ knots
- 199 2. Skew- t marginal, $K = 1$ knots, $T = -\infty$
- 200 3. Symmetric- t marginal, $K = 1$ knots, $T = q(0.80)$
- 201 4. Skew- t marginal, $K = 5$ knots, $T = -\infty$
- 202 5. Symmetric- t marginal, $K = 5$ knots, $T = q(0.80)$
- 203 6. A max-stable model based on Reich and Shaby (2012) thresholded at $T = q(0.80)$

204 where $q(0.80)$ is the 80th sample quantile of the data. The design matrix \mathbf{X} includes an intercept with a first-
 205 order spatial trend with priors of $\beta_{\text{int}}, \beta_{\text{lat}}, \beta_{\text{long}}, \stackrel{iid}{\sim} \mathcal{N}(0, 10)$. The spatial covariance parameters have priors
 206 $\log(\nu) \sim \mathcal{N}(-1.2, 1), \gamma \sim \text{Unif}(0, 1), \rho \sim \text{Unif}(15)$. The skewness parameter has prior $\lambda_2 \sim \text{IG}(0.1, 0.1)$.

207 The residual variance terms have priors $\sigma_t^2(\mathbf{s}) \sim \text{IG}(0.1, 0.1)$. The knots have priors $\mathbf{w} \sim \text{Unif}(\mathcal{D})$. We tried
 208 also fitting the skew- t marginals for the thresholded models, but it is very challenging for the MCMC to
 209 properly identify the skewness parameter with a censored left tail. Each chain of the MCMC ran for 20,000
 210 iterations with a burn-in period of 10,000 iterations. Parameters appear to converge properly; however, in
 211 the models with multiple partitions (i.e. models 4 and 5) it is hard to assess the convergence of \mathbf{w} , $z(\mathbf{s})$, and
 212 $\sigma^2(\mathbf{s})$ because of partition label switching throughout the MCMC.

213 5.2 Cross validation

214 Models were compared using cross validation with 100 sites used as training sites and 44 sites withheld for
 215 testing. The model was fit using the training set, and predictions were generated at the testing site locations.
 216 Because one of the primary goals of this model is to predict exceedances over a fixed threshold, we use Brier
 217 scores to select the model that best fits the data (Gneiting and Raftery, 2007). The Brier score for predicting
 218 exceedance of a threshold c is given by $[e(c) - P(c)]^2$ where $e(c) = I[y > c]$ is an indicator function
 219 indicating that a test set value, y , has exceeded the threshold, c , and $P(c)$ is the predicted probability of
 220 exceeding c . We average the Brier scores over all test sites and days. For the Brier score, a lower score
 221 indicates a better fit.

222 5.3 Results

223 We compared the Brier scores for exceeding 4 different thresholds for each dataset. The thresholds used for
 224 the Brier scores are extreme quantiles from the simulated data for $q(0.90)$, $q(0.95)$, $q(0.98)$, and $q(0.99)$.
 225 Figure 2 gives the Brier score relative to the Brier score for the Gaussian method calculated as

$$\text{BS}_{\text{rel}} = \frac{\text{BS}_{\text{method}}}{\text{BS}_{\text{Gaussian}}}. \quad (20)$$

226 We analyzed the results for the simulation study using a Friedman test at $\alpha = 0.05$ to see if at least one
227 method had a significantly different Brier score. For Friedman tests that came back with a significant p-
228 value, we conducted a Wilcoxon-Nemenyi-McDonald-Thompson test to see which of the methods had dif-
229 ferent results. The full results for the Wilcoxon-Nemenyi-McDonald-Thompson tests are given in Appendix
230 A.5.

231 Figure 2 shows that when the data come from a Gaussian process, our methods perform comparably to
232 the Gaussian method. For data settings with skew- t marginals (settings 2 – 3), we find significant improve-
233 ment over the Gaussian method. Furthermore in these data settings, we find the best performance occurs
234 when the number of knots used in the method matches the number of knots used for data generation. The
235 non-thresholded methods tend to outperform the thresholded methods, but this is not surprising given that
236 in most cases, the data are generated directly from the model used in the method. For the max-stable data,
237 we see that for low-extreme quantiles, the Gaussian method performs better, for more extreme quantiles, the
238 single-partition method, both thresholded and non-thresholded, perform significantly better than the Gaus-
239 sian. Finally, for setting 5, although the thresholded version of the single-partition model tends to perform
240 the best across all of the extreme quantiles, the difference between the thresholded and non-thresholded
241 methods is no longer significant in the more extreme quantiles. In summary, our method provides more flex-
242 ibility for data that demonstrate some level of asymmetry or heavy tails, while still performing comparably
243 to Gaussian methods when the data are symmetric and have light tails.

244 **6 Data analysis**

245 To illustrate this method, we consider the daily maximum 8-hour ozone measurements for July 1 - 31, 2005
246 at 1089 Air Quality System (AQS) monitoring sites in the United States as the response (see Figure 3). For
247 each site, we also have covariate information containing the estimated ozone from the Community Multi-

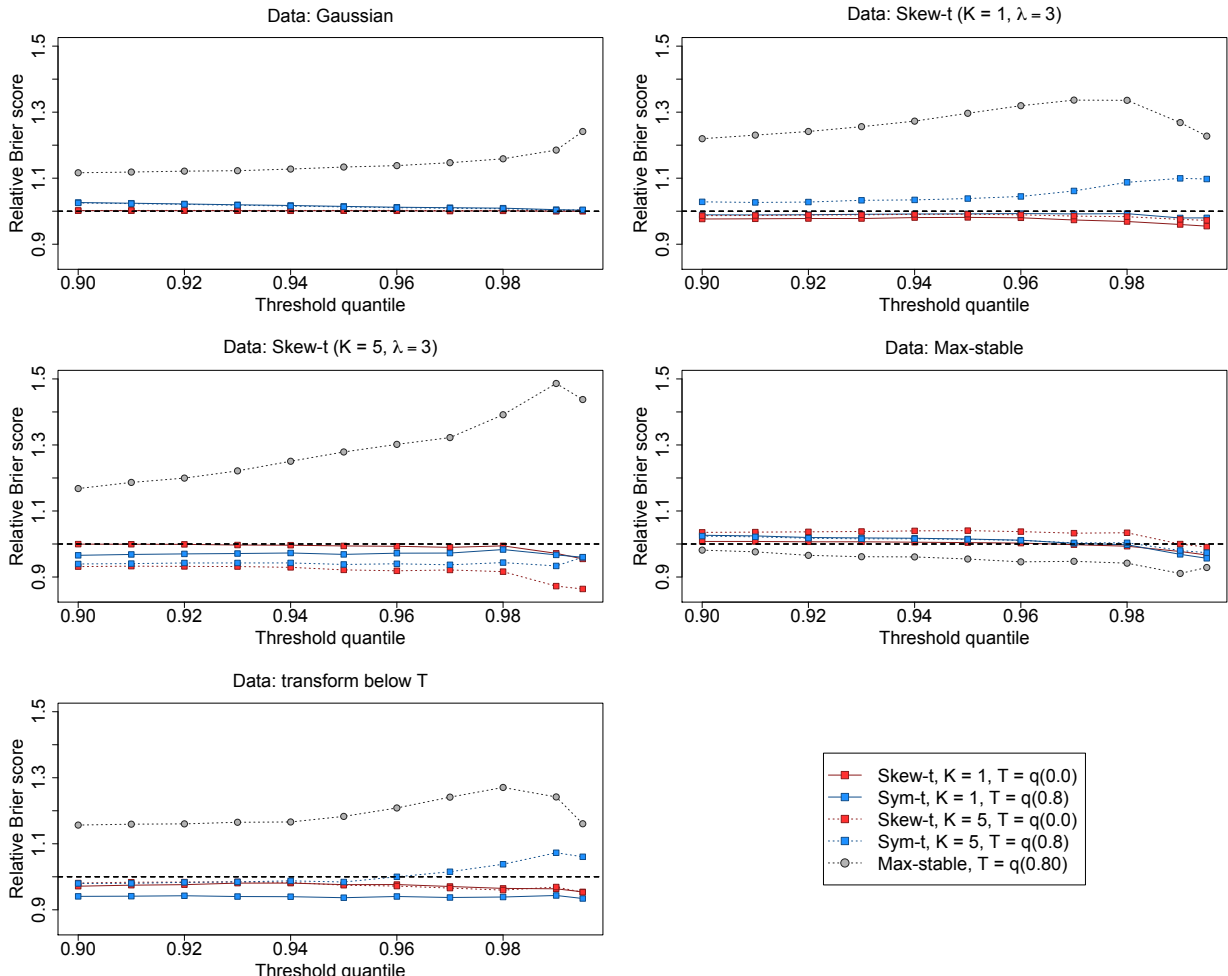


Figure 2: Brier scores relative to the Gaussian method for simulation study results. A ratio lower than 1 indicates that the method outperforms the Gaussian method.

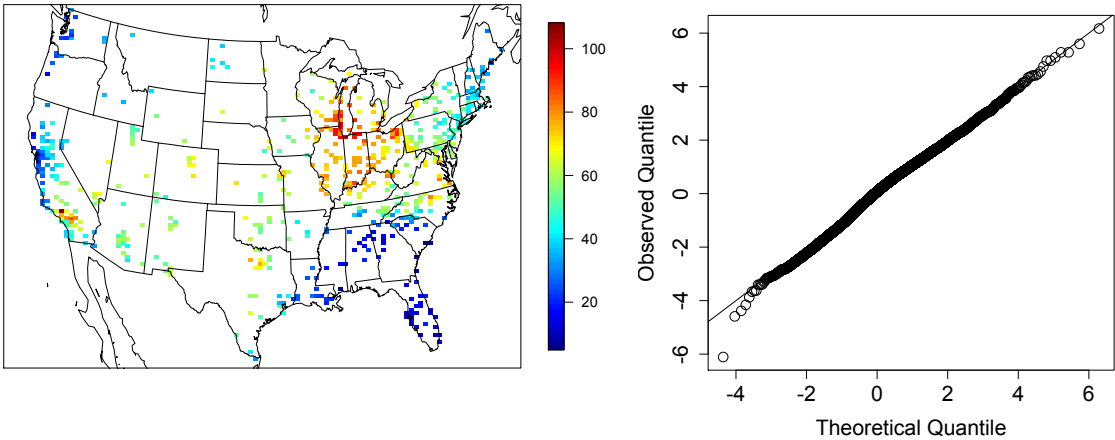


Figure 3: Ozone values on 10 July 2005 (left) Q-Q plot of the residuals (right)

248 scale Air Quality (CMAQ) modeling system. Initially, we fit a linear regression assuming a mean function
 249 of

$$\mathbf{X}_t^T(\mathbf{s})\boldsymbol{\beta} = \beta_0 + \beta_1 \cdot \text{CMAQ}_t(\mathbf{s}). \quad (21)$$

250 The data from July 10 are shown in Figure 3 along with a Q-Q plot of the residuals compared to a skew-*t*
 251 distribution with 10 d.f. and $\alpha = 1$. Exploratory data analysis indicates that there is dependence in the high
 252 quantile levels of the residuals beyond what we expect in the case of independence.

253 **6.1 Model comparisons**

254 We fit the model using Gaussian and skew-*t* marginal distributions with $K = 1, 5, 6, 7, 8, 9, 10, 15$ partitions.
 255 We choose to censor $Y(\mathbf{s})$ at $T = 0, 50$ (0.42 sample quantile), and 75 (0.92 sample quantile) ppb in order
 256 to compare results from no, moderate, and high censoring. The upper threshold of 75 ppb was used because
 257 the current air quality standard is based on exceedance of 75 ppb. As with the simulation study, for models
 258 with a threshold of $T = 75$, we use a symmetric-*t* marginal distribution. We also compare models with no

259 time series to models that include the time series. Finally, as a comparison to max-stable methods, we fit
260 the model using the hierarchical max-stable model of Reich and Shaby (2012) with the data thresholded at
261 $T = 75$. All methods assume the mean function given in (21). To ensure that the max-stable method runs
262 in a reasonable amount of time, we take a stratified sample of the sites to get 800 sites and consider this
263 our new dataset. We conduct two-fold cross validation using 400 training sites and 400 validation sites as
264 described in Section 5.2

265 Each chain of the MCMC ran for 30000 iterations with a burn-in period of 25000 iterations. Parameters
266 appear to converge properly; however, as before, for models with multiple partitions it is hard to assess the
267 convergence of \mathbf{w} , $z(\mathbf{s})$, and $\sigma^2(\mathbf{s})$ because of partition label switching throughout the MCMC. For each
268 model, Brier scores were averaged over all sites and days to obtain a single Brier score for each dataset. At
269 a particular threshold or quantile level, the model that fits the best is the one with the lowest score. We then
270 compute the relative (to Gaussian) Brier scores (see Section 5.3) to compare each model.

271 6.2 Results

272 The results suggest that the skew- t , thresholded, partitioned, and time series models all give an improvement
273 in predictions over the Gaussian model, whereas the max-stable method results in relative Brier scores
274 between 1.07 and 1.15 indicating poorer performance than the Gaussian model. The plots in Figure 4
275 show the relative Brier scores for time-series and non-time-series models, using $K = 1, 7$, and 15 knots at
276 thresholds $T = 0, 50$, and 75 ppb. Most of the models perform similarly across all the Brier scores; however,
277 for single-partition models without thresholding, performance tends to diminish in the extreme quantiles.
278 The results also suggest that thresholding improves performance for estimates in the extreme quantiles. Both
279 plots have similar features suggesting that most settings do reasonably well. In particular, for all extreme
280 quantiles, selecting a moderate number of knots (e.g. $K = 5, \dots, 10$) tends to give the best results. Table 1

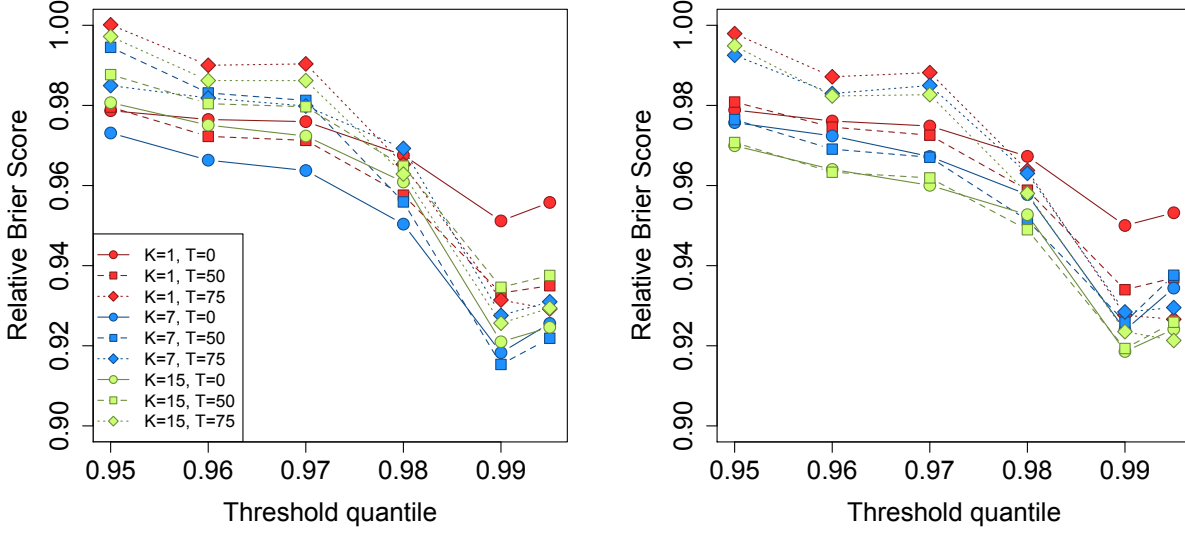


Figure 4: Relative Brier scores for time-series models (left) and non-time-series models (right). Relative brier score for the max-stable model is between 1.07 and 1.15

281 shows the best two models for selected extreme quantiles.

282 We illustrate the predictive capability of our model in Figure 6 by plotting the 99th quantile of the
283 posterior predictive density for July in South Carolina and Georgia. We fit the model using four methods,
284 two reference and two that performed better. These four methods are

- 285 1. Gaussian (reference)
- 286 2. Skew- t , $K = 1$ knot, $T = 0$, no time series (reference)
- 287 3. Skew- t , $K = 5$ knots, $T = 50$, no time series (comparison)
- 288 4. Symmetric- t , $K = 10$ knots, $T = 75$, time series (comparison).

289 In the bottom two plots, we plot the differences between method 4 and methods 1 and 2. The most noticeable
290 differences between the reference methods and the comparison methods is that the comparison methods tend
291 to give higher estimates of the 99th quantile along the I-85 corridor between Charlotte and Atlanta.

292 NEED TO ADD STUFF HERE ACKNOWLEDGING THAT MARGINALS ARE DIFFERENT Also,

Table 1: Top two performing models for ozone analysis at extreme quantiles with Relative Brier score

		1st				2nd		
$q(0.90)$	No time series	$K = 7$	$T = 0$	BS: 0.980	No time series	$K = 9$	$T = 0$	BS: 0.980
$q(0.95)$	No time series	$K = 15$	$T = 50$	BS: 0.970	No time series	$K = 9$	$T = 50$	BS: 0.970
$q(0.98)$	No time series	$K = 5$	$T = 50$	BS: 0.945	No time series	$K = 10$	$T = 50$	BS: 0.946
$q(0.99)$	Time series	$K = 10$	$T = 75$	BS: 0.912	Time series	$K = 6$	$T = 75$	BS: 0.913
$q(0.995)$	Time series	$K = 6$	$T = 75$	BS: 0.917	Time series	$K = 10$	$T = 75$	BS: 0.918

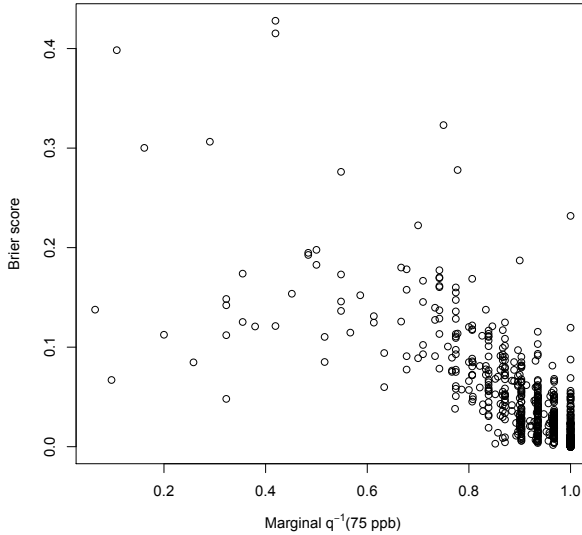


Figure 5: Comparison of Brier score performance by marginal quantile representing 75ppb

293 add an explanation about the purpose of the plot in 5

294 7 Discussion

295 In this paper we propose a new threshold exceedance approach for spatiotemporal modeling based on the
 296 skew- t process. The proposed model gives flexible tail behavior, demonstrates asymptotic dependence for
 297 observations at sites that are near to one another, and has computation on the order of Gaussian models
 298 for large space-time datasets. In the simulation study, we demonstrate that this model shows statistically
 299 significant improvements over a naïve Gaussian approach. In both the simulation study, and the application
 300 to ozone data, we find that incorporating a partition in the model improves extreme prediction. Furthermore

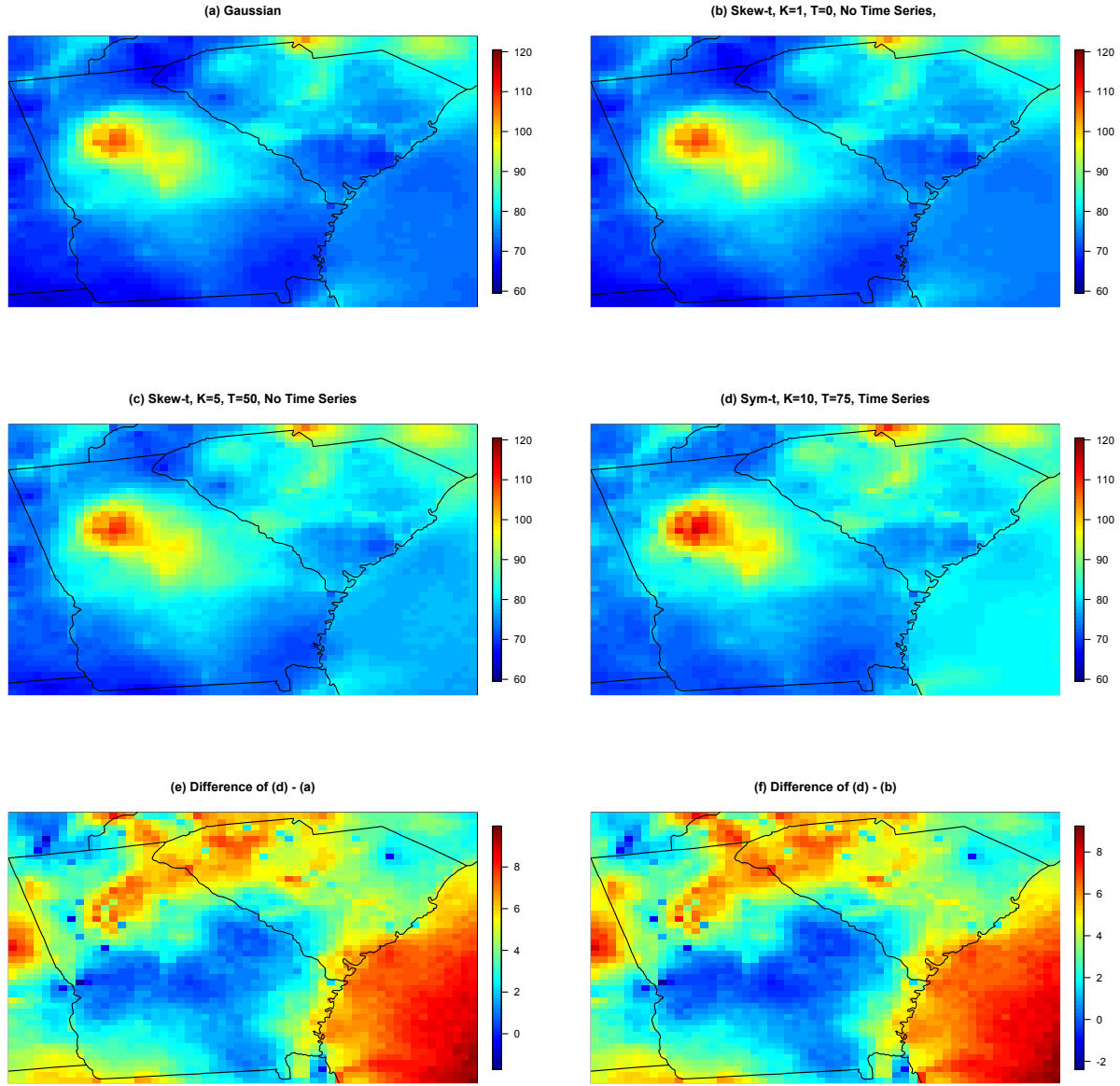


Figure 6: (a) – (d) give the posterior predictive $\hat{q}(0.99)$ for the month of July under four different models, (e) gives the difference between $\hat{q}(0.99)$ in plots (d) and (a), (f) gives the difference between $\hat{q}(0.99)$ in plots (d) and (b).

301 the results from the data analysis suggest that thresholding can improve performance when predicting in the
302 extreme tails of the data.

303 This model presents new avenues for future research. One possibility is the implementation of a different
304 partition structure. We choose to define the random effects for a site by using an indicator function based on
305 closeness to a knot. However, this indicator function could be replaced by kernel function that would allow
306 for multiple knots to impact each site, with the weight of each knot to be determined by some characteristic
307 such as distance. Another area that should be explored is the temporal dependence in the model. Instead of
308 implementing a time series on the random effects, a three-dimensional covariance structure on the residuals
309 could be implemented to address temporal dependence. Finally, we acknowledge that by specifying the
310 number of knots, we may be underestimating the uncertainty in the model. This could be incorporated by
311 treating the number of knots as a model parameter instead of fixing it to be a specific value.

312 **Acknowledgments**

313 **A Appendices**

314 **A.1 MCMC details**

315 The MCMC sampling for the model 4 is done using R (<http://www.r-project.org>). Whenever possible,
316 we select conjugate priors (see Appendix A.2); however, for some of the parameters, no conjugate prior
317 distributions exist. When no conjugate prior distribution exists, we use a random walk Metropolis Hastings
318 update step. In each Metropolis Hastings update, we tune the algorithm to give acceptance rates near 0.40.

319 **Spatial knot locations**

320 For each day, we update the spatial knot locations, $\mathbf{w}_1, \dots, \mathbf{w}_K$, using a Metropolis Hastings block up-
 321 date. Because the spatial domain is bounded, we generate candidate knots using the transformed knots
 322 $\mathbf{w}_1^*, \dots, \mathbf{w}_K^*$ (see section 3.3) and a random walk bivariate Gaussian candidate distribution

$$\mathbf{w}_k^{*(c)} \sim N(\mathbf{w}_k^{*(r-1)}, s^2 I_2)$$

323 where $\mathbf{w}_k^{*(r-1)}$ is the location for the transformed knot at MCMC iteration $r - 1$, s is a tuning parameter,
 324 and I_2 is an identity matrix. After candidates have been generated for all K knots, the acceptance ratio is

$$R = \left\{ \frac{l[Y_t(\mathbf{s}|\mathbf{w}_1^{(c)}, \dots, \mathbf{w}_K^{(c)}, \dots)]}{l[Y_t(\mathbf{s}|\mathbf{w}_1^{(r-1)}, \dots, \mathbf{w}_K^{(r-1)}, \dots)]} \right\} \times \left\{ \frac{\prod_{k=1}^K \phi(\mathbf{w}_k^{(c)})}{\prod_{k=1}^K \phi(\mathbf{w}_k^{(r-1)})} \right\} \times \left\{ \frac{\prod_{k=1}^K p(\mathbf{w}_k^{*(c)})}{\prod_{k=1}^K p(\mathbf{w}_k^{*(r-1)})} \right\}$$

325 where l is the likelihood given in (18), and $p(\cdot)$ is the prior either taken from the time series given in (3.3)
 326 or assumed to be uniform over \mathcal{D} . The candidate knots are accepted with probability $\min\{R, 1\}$.

327 **Spatial random effects**

328 If there is no temporal dependence amongst the observations, we use a Gibbs update for z_{tk} , and the posterior
 329 distribution is given in A.2. If there is temporal dependence amongst the observations, then we update z_{tk}
 330 using a Metropolis Hastings update. Because this model uses $|z_{tk}|$, we generate candidate random effects
 331 using the z_{tk}^* (see Section 3.3) and a random walk Gaussian candidate distribution

$$z_{tk}^{*(c)} \sim N(z_{tk}^{*(r-1)}, s^2)$$

332 where $z_{tk}^{*(r-1)}$ is the value at MCMC iteration $r - 1$, and s is a tuning parameter. The acceptance ratio is

$$R = \left\{ \frac{l[Y_t(\mathbf{s})|z_{tk}^{(c)}, \dots]}{l[Y_t(\mathbf{s})|z_{tk}^{(r-1)}]} \right\} \times \left\{ \frac{p[z_{tk}^{(c)}]}{p[z_{tk}^{(r-1)}]} \right\}$$

333 where $p[\cdot]$ is the prior taken from the time series given in Section 3.3. The candidate is accepted with
 334 probability $\min\{R, 1\}$.

335 Variance terms

336 When there is more than one site in a partition, then we update σ_{tk}^2 using a Metropolis Hastings update.
 337 First, we generate a candidate for σ_{tk}^2 using an $IG(a^*/s, b^*/s)$ candidate distribution in an independence
 338 Metropolis Hastings update where $a^* = (n_{tk} + 1)/2 + a$, $b^* = [Y_{tk}^T \Sigma_{tk}^{-1} Y_{tk} + z_{tk}^2]/2 + b$, n_{tk} is the number
 339 of sites in partition k on day t , and Y_{tk} and Σ_{tk}^{-1} are the observations and precision matrix for partition k on
 340 day t . The acceptance ratio is

$$R = \left\{ \frac{l[Y_t(\mathbf{s})|\sigma_{tk}^{2(c)}, \dots]}{l[Y_t(\mathbf{s})|\sigma_{tk}^{2(r-1)}]} \right\} \times \left\{ \frac{l[z_{tk}|\sigma_{tk}^{2(c)}, \dots]}{l[z_{tk}|\sigma_{tk}^{2(r-1)}, \dots]} \right\} \times \left\{ \frac{p[\sigma_{tk}^{2(c)}]}{p[\sigma_{tk}^{2(r-1)}]} \right\} \times \left\{ \frac{c[\sigma_{tk}^{2(r-1)}]}{c[\sigma_{tk}^{2(c)}]} \right\}$$

341 where $p[\cdot]$ is the prior either taken from the time series given in Section 3.3 or assumed to be $IG(a, b)$, and
 342 $c[\cdot]$ is the candidate distribution. The candidate is accepted with probability $\min\{R, 1\}$.

343 Spatial covariance parameters

344 We update the three spatial covariance parameters, $\log(\rho)$, $\log(\nu)$, γ , using a Metropolis Hastings block
 345 update step. First, we generate a candidate using a random walk Gaussian candidate distribution

$$\log(\rho)^{(c)} \sim N(\log(\rho)^{(r-1)}, s^2)$$

³⁴⁶ where $\log(\rho)^{(r-1)}$ is the value at MCMC iteration $r - 1$, and s is a tuning parameter. Candidates are
³⁴⁷ generated for $\log(\nu)$ and γ in a similar fashion. The acceptance ratio is

$$R = \left\{ \frac{\prod_{t=1}^T l[Y_t(\mathbf{s}) | \rho^{(c)}, \nu^{(c)}, \gamma^{(c)}, \dots]}{\prod_{t=1}^T l[Y_t(\mathbf{s}) | \rho^{(r-1)}, \nu^{(r-1)}, \gamma^{(r-1)}, \dots]} \right\} \times \left\{ \frac{p[\rho^{(c)}]}{p[\rho^{(r-1)}]} \right\} \times \left\{ \frac{p[\nu^{(c)}]}{p[\nu^{(r-1)}]} \right\} \times \left\{ \frac{p[\gamma^{(c)}]}{p[\gamma^{(r-1)}]} \right\}.$$

³⁴⁸ All three candidates are accepted with probability $\min\{R, 1\}$.

³⁴⁹ A.2 Posterior distributions

³⁵⁰ **Conditional posterior of $z_{tk} | \dots$**

³⁵¹ If knots are independent over days, then the conditional posterior distribution of $|z_{tk}|$ is conjugate. For
³⁵² simplicity, drop the subscript t , let $\tilde{z}_{tk} = |z_{tk}|$, and define

$$R(\mathbf{s}) = \begin{cases} Y(\mathbf{s}) - X(\mathbf{s})\beta & s \in P_l \\ Y(\mathbf{s}) - X(\mathbf{s})\beta - \lambda \tilde{z}(\mathbf{s}) & s \notin P_l \end{cases}$$

³⁵³ Let

$R_1 = \text{the vector of } R(\mathbf{s}) \text{ for } s \in P_l$

$R_2 = \text{the vector of } R(\mathbf{s}) \text{ for } s \notin P_l$

$$\Omega = \Sigma^{-1}.$$

³⁵⁴ Then

$$\begin{aligned}\pi(z_l | \dots) &\propto \exp \left\{ -\frac{1}{2} \left[\begin{pmatrix} R_1 - \lambda \tilde{z}_l \mathbf{1} \\ R_2 \end{pmatrix}^T \begin{pmatrix} \Omega_{11} & \Omega_{12} \\ \Omega_{21} & \Omega_{22} \end{pmatrix} \begin{pmatrix} R_1 - \lambda \tilde{z}_l \mathbf{1} \\ R_2 \end{pmatrix} + \frac{\tilde{z}_l^2}{\sigma_l^2} \right] \right\} I(z_l > 0) \\ &\propto \exp \left\{ -\frac{1}{2} [\Lambda_l \tilde{z}_l^2 - 2\mu_l \tilde{z}_l] \right\}\end{aligned}$$

³⁵⁵ where

$$\begin{aligned}\mu_l &= \lambda(R_1^T \Omega_{11} + R_2^T \Omega_{21}) \mathbf{1} \\ \Lambda_l &= \lambda^2 \mathbf{1}^T \Omega_{11} \mathbf{1} + \frac{1}{\sigma_l^2}.\end{aligned}$$

³⁵⁶ Then $\tilde{Z}_l | \dots \sim N_{(0, \infty)}(\Lambda_l^{-1} \mu_l, \Lambda_l^{-1})$

³⁵⁷ **Conditional posterior of β | ...**

³⁵⁸ Let $\beta \sim N_p(0, \Lambda_0)$ where Λ_0 is a precision matrix. Then

$$\begin{aligned}\pi(\beta | \dots) &\propto \exp \left\{ -\frac{1}{2} \beta^T \Lambda_0 \beta - \frac{1}{2} \sum_{t=1}^T [\mathbf{Y}_t - X_t \beta - \lambda |z_t|]^T \Omega [\mathbf{Y}_t - X_t \beta - \lambda |z_t|] \right\} \\ &\propto \exp \left\{ -\frac{1}{2} \left[\beta^T \Lambda_\beta \beta - 2 \sum_{t=1}^T [\beta^T X_t^T \Omega (\mathbf{Y}_t - \lambda |z_t|)] \right] \right\} \\ &\propto N(\Lambda_\beta^{-1} \mu_\beta, \Lambda_\beta^{-1})\end{aligned}$$

³⁵⁹ where

$$\begin{aligned}\mu_\beta &= \sum_{t=1}^T [X_t^T \Omega (\mathbf{Y}_t - \lambda |z_t|)] \\ \Lambda_\beta &= \Lambda_0 + \sum_{t=1}^T X_t^T \Omega X_t.\end{aligned}$$

³⁶⁰ **Conditional posterior of $\sigma^2 | \dots$**

³⁶¹ In the case where $L = 1$ and temporal dependence is negligible, then σ^2 has a conjugate posterior distribution. Let $\sigma_t^2 \stackrel{iid}{\sim} \text{IG}(\alpha_0, \beta_0)$. For simplicity, drop the subscript t . Then

$$\begin{aligned}\pi(\sigma^2 | \dots) &\propto (\sigma^2)^{-\alpha_0-1/2-n/2-1} \exp \left\{ -\frac{\beta_0}{\sigma^2} - \frac{|z|^2}{2\sigma^2} - \frac{(\mathbf{Y} - \boldsymbol{\mu})^T \Sigma^{-1} (\mathbf{Y} - \boldsymbol{\mu})}{2\sigma^2} \right\} \\ &\propto (\sigma^2)^{-\alpha_0-1/2-n/2-1} \exp \left\{ -\frac{1}{\sigma^2} \left[\beta_0 + \frac{|z|^2}{2} + \frac{1}{2} (\mathbf{Y} - \boldsymbol{\mu})^T \Sigma^{-1} (\mathbf{Y} - \boldsymbol{\mu}) \right] \right\} \\ &\propto \text{IG}(\alpha^*, \beta^*)\end{aligned}$$

³⁶³ where

$$\begin{aligned}\alpha^* &= \alpha_0 + \frac{1}{2} + \frac{n}{2} \\ \beta^* &= \beta_0 + \frac{|z|^2}{2} + \frac{1}{2} (\mathbf{Y} - \boldsymbol{\mu})^T \Sigma^{-1} (\mathbf{Y} - \boldsymbol{\mu}).\end{aligned}$$

³⁶⁴ In the case that $L > 1$, a random walk Metropolis Hastings step will be used to update σ_{lt}^2 .

365 Conditional posterior of $\lambda | \dots$

366 For convergence purposes we model $\lambda = \lambda_1 \lambda_2$ where

$$\lambda_1 = \begin{cases} +1 & \text{w.p.0.5} \\ -1 & \text{w.p.0.5} \end{cases} \quad (22)$$

$$\lambda_2^2 \sim IG(\alpha_\lambda, \beta_\lambda). \quad (23)$$

$$(24)$$

367 Then

$$\begin{aligned} \pi(\lambda_2 | \dots) &\propto \lambda_2^{2(-\alpha_\lambda-1)} \exp\left\{-\frac{\beta_\lambda}{\lambda_2^2}\right\} \prod_{t=1}^T \prod_{k=1}^K \frac{1}{\lambda_2} \exp\left\{-\frac{z_{tk}^2}{2\lambda_2^2 \sigma_{tk}^2}\right\} \\ &\propto \lambda_2^{2(-\alpha_\lambda-kt-1)} \exp\left\{-\frac{1}{\lambda_2^2} \left[\beta_\lambda + \frac{z^2}{2\sigma_{tk}^2}\right]\right\} \end{aligned}$$

368 Then $\lambda_2 | \dots \sim IG(\alpha_\lambda + kt, \beta_\lambda + \frac{z^2}{2\sigma_{tk}^2})$

369 **A.3 Proof that** $\lim_{h \rightarrow \infty} \pi(h) = 0$

370 Let $N(A)$ be the number of knots in A , the area between sites \mathbf{s}_1 and \mathbf{s}_2 . Consider a spatial Poisson process

371 with intensity $\mu(A)$. So,

$$P[N(A) = k] = \frac{\mu(A)^k \exp\{-\mu(A)\}}{k!}.$$

372 Then for any finite k , $\lim_{h \rightarrow \infty} P[N(A) = k] = 0$ because $\lim_{h \rightarrow \infty} \mu(A) = \infty$. With each additional knot

373 in A , the chance that \mathbf{s}_1 and \mathbf{s}_2 will be in the same partition will decrease, because partition membership

374 is defined by the closest knot to a site. Therefore, $\lim_{h \rightarrow \infty} \pi(h) = 0$.

375 **A.4 Skew- t distribution**

376 **Univariate extended skew- t distribution**

377 We say that Y follow a univariate extended skew- t distribution with location $\xi \in \mathcal{R}$, scale $\omega > 0$, skew

378 parameter $\alpha \in \mathcal{R}$, extended parameter $\tau \in \mathcal{R}$, and degrees of freedom ν if has distribution function

$$f_{\text{EST}}(y) = \omega^{-1} \frac{f_T(z; \nu)}{F_T(\tau/\sqrt{1+\alpha^2}; \nu)} F_T \left[(\alpha z + \tau) \sqrt{\frac{\nu+1}{\nu+z^2}}; 0, 1, \nu+1 \right] \quad (25)$$

379 where $f_T(t; \nu)$ is a univariate Student's t with ν degrees of freedom, $F_T(t; \nu) = P(T < t)$, and $z = (y - \xi)/\omega$.

380 In the case that $\tau = 0$, then Y follows a univariate skew- t distribution.

381 **Multivariate skew- t distribution**

382 If $\mathbf{Z} \sim \text{ST}_d(0, \bar{\Omega}, \boldsymbol{\alpha}, \eta)$ is a d -dimensional skew- t distribution, and $\mathbf{Y} = \xi + \boldsymbol{\omega}\mathbf{Z}$, where $\boldsymbol{\omega} = \text{diag}(\omega_1, \dots, \omega_d)$,

383 then the density of Y at y is

$$f_y(\mathbf{y}) = \det(\boldsymbol{\omega})^{-1} f_z(\mathbf{z}) \quad (26)$$

384 where

$$f_z(\mathbf{z}) = 2t_d(\mathbf{z}; \bar{\Omega}, \eta) T \left[\boldsymbol{\alpha}^T \mathbf{z} \sqrt{\frac{\eta+d}{\nu+Q(\mathbf{z})}}; \eta+d \right] \quad (27)$$

$$\mathbf{z} = \boldsymbol{\omega}^{-1}(\mathbf{y} - \xi) \quad (28)$$

385 where $t_d(\mathbf{z}; \bar{\Omega}, \eta)$ is a d -dimensional Student's t -distribution with scale matrix $\bar{\Omega}$ and degrees of freedom

386 η , $Q(\mathbf{z}) = \mathbf{z}^T \bar{\Omega}^{-1} \mathbf{z}$ and $T(\cdot; \eta)$ denotes the univariate Student's t distribution function with η degrees of

387 freedom (Azzalini and Capitanio, 2014).

388 **Extremal dependence**

389 For a bivariate skew- t random variable $\mathbf{Y} = [Y(\mathbf{s}), Y(\mathbf{t})]^T$, the $\chi(h)$ statistic (Padoan, 2011) is given by

$$\chi(h) = \bar{F}_{\text{EST}} \left\{ \frac{[x_1^{1/\eta} - \varrho(h)]\sqrt{\eta+1}}{\sqrt{1-\varrho(h)^2}}; 0, 1, \alpha_1, \tau_1, \eta + 1 \right\} + \bar{F}_{\text{EST}} \left\{ \frac{[x_2^{1/\eta} - \varrho(h)]\sqrt{\eta+1}}{\sqrt{1-\varrho(h)^2}}; 0, 1, \alpha_2, \tau_2, \eta + 1 \right\}, \quad (29)$$

390 where \bar{F}_{EST} is the univariate survival extended skew- t function with zero location and unit scale, $\varrho(h) = \text{cor}(y_1, y_2)$,

391 $\alpha_j = \alpha_i \sqrt{1 - \varrho^2}$, $\tau_j = \sqrt{\eta+1}(\alpha_j + \alpha_i \varrho)$, and $x_j = F_T(\bar{\alpha}_i \sqrt{\eta+1}; 0, 1, \eta)/F_T(\bar{\alpha}_j \sqrt{\eta+1}; 0, 1, \eta)$ with

392 $j = 1, 2$ and $i = 2, 1$ and where $\bar{\alpha}_j = (\alpha_j + \alpha_i \varrho)/\sqrt{1 + \alpha_i^2[1 - \varrho(h)^2]}$.

393 **Proof that** $\lim_{h \rightarrow \infty} \chi(h) > 0$

394 Consider the bivariate distribution of $\mathbf{Y} = [Y(\mathbf{s}), Y(\mathbf{t})]^T$, with $\varrho(h)$ given by (3). So, $\lim_{h \rightarrow \infty} \varrho(h) = 0$.

395 Then

$$\lim_{h \rightarrow \infty} \chi(h) = \bar{F}_{\text{EST}} \left\{ \sqrt{\eta+1}; 0, 1, \alpha_1, \tau_1, \eta + 1 \right\} + \bar{F}_{\text{EST}} \left\{ \sqrt{\eta+1}; 0, 1, \alpha_2, \tau_2, \eta + 1 \right\}. \quad (30)$$

396 Because the extended skew- t distribution is not bounded above, for all $\bar{F}_{\text{EST}}(x) = 1 - F_{\text{EST}} > 0$ for all

397 $x < \infty$. Therefore, for a skew- t distribution, $\lim_{h \rightarrow \infty} \chi(h) > 0$.

398 **A.5 Simulation study pairwise difference results**

399 The following tables show the methods that have significantly different Brier scores when using a Wilcoxon-

400 Nemenyi-McDonald-Thompson test. In each column, different letters signify that the methods have signifi-

401 cantly different Brier scores. For example, there is significant evidence to suggest that method 1 and method

402 4 have different Brier scores at $q(0.90)$, whereas there is not significant evidence to suggest that method 1

403 and method 2 have different Brier scores at $q(0.90)$. In each table group A represents the group with the
 404 lowest Brier scores. Groups are significant with a familywise error rate of $\alpha = 0.05$.

Table 2: Setting 1 – Gaussian marginal, $K = 1$ knot

	$q(0.90)$	$q(0.95)$	$q(0.98)$	$q(0.99)$
Method 1	A	A	A	A
Method 2	A	A	A	A
Method 3	B	B	C	A
Method 4	A	A	A B	A
Method 5	B	B	B C	A
Method 6	C	C	D	B

Table 3: Setting 2 – Skew- t marginal, $K = 1$ knot

	$q(0.90)$	$q(0.95)$	$q(0.98)$	$q(0.99)$
Method 1	C	B	B C	B
Method 2	A	A	A	A
Method 3	B C	A B	A B	A B
Method 4	A B	B	B	A
Method 5	D	C	C	B
Method 6	E	D	D	C

Table 4: Setting 3 – Skew- t marginal, $K = 5$ knots

	$q(0.90)$	$q(0.95)$	$q(0.98)$	$q(0.99)$
Method 1	B	C	B	B
Method 2	B	C	B	B
Method 3	A	B	B	B
Method 4	A	A	A	A
Method 5	A	A	A	A
Method 6	C	D	C	C

405 References

- 406 Azzalini, A. and Capitanio, A. (2014) *The Skew-Normal and Related Families*. Institute of Mathematical Statistics Monographs. Cambridge University Press.
 407 URL <https://books.google.com/books?id=-tkaAgAAQBAJ>.
- 408
- 409 Coles, S., Heffernan, J. and Tawn, J. (1999) Dependence Measures for Extreme Value Analyses. *Extremes*,
 410 2, 339–365. URL <http://link.springer.com/article/10.1023/A:1009963131610>.

Table 5: Setting 4 – Max-stable

	$q(0.90)$	$q(0.95)$	$q(0.98)$	$q(0.99)$
Method 1	A B	B	B	C
Method 2	B	B	B	B C
Method 3	C D	C	B	B
Method 4	D	C	C	B C
Method 5	C	C	B	B C
Method 6	A	A	A	A

Table 6: Setting 5 – Transformation below $T = q(0.80)$

	$q(0.90)$	$q(0.95)$	$q(0.98)$	$q(0.99)$
Method 1	C	B	C	C
Method 2	B	B	B	A B
Method 3	A	A	A	A
Method 4	B C	B	B	B C
Method 5	B	B	B C	C
Method 6	D	C	D	D

- 411 Davison, A. C. and Smith, R. L. (1990) Models for exceedances over high thresholds (with Discussion).
412 *Journal of the Royal Statistical Society. Series B (Methodological)*, **52**, 393–442.
- 413 Engelke, S., Malinowski, A., Kabluchko, Z. and Schlather, M. (2014) Estimation of Hüsler-Reiss distributions
414 and Brown-Resnick processes. *Journal of the Royal Statistical Society. Series B: Statistical Methodology*, 239–265.
- 415
- 416 Genton, M. G. (2004) *Skew-Elliptical Distributions and Their Applications: A Journey Beyond Normality*. Statistics (Chapman & Hall/CRC). Taylor & Francis.
417 URL <http://books.google.com/books?id=R9hBnwEACAAJ>.
- 418
- 419 Gneiting, T. and Raftery, A. E. (2007) Strictly Proper Scoring Rules, Prediction,
420 and Estimation. *Journal of the American Statistical Association*, **102**, 359–378.
421 URL <http://www.tandfonline.com/doi/abs/10.1198/016214506000001437>.
- 422 Huser, R. and Davison, A. C. (2014) Space-time modelling of extreme
423 events. *Journal of the Royal Statistical Society: Series B (Statistical
424 Methodology)*, **76**, 439–461. URL <http://arxiv.org/abs/1201.3245>
425 <http://doi.wiley.com/10.1111/rssb.12035>.
- 426 Kim, H.-M., Mallick, B. K. and Holmes, C. C. (2005) Analyzing Nonstationary Spatial Data Using Piece-
427 wise Gaussian Processes. *Journal of the American Statistical Association*, **100**, 653–668.
- 428 Ledford, A. W. and Tawn, J. a. (1996) Statistics for near independence in multivariate extreme values.
429 *Biometrika*, **83**, 169–187.
430 URL <http://biomet.oxfordjournals.org/cgi/content/abstract/83/1/169>.
- 431 Padoan, S. A. (2011) Multivariate extreme models based on underlying skew-

- 432 and skew-normal distributions. *Journal of Multivariate Analysis*, **102**, 977–991.
433 URL`http://linkinghub.elsevier.com/retrieve/pii/S0047259X11000157.`
- 434 Padoan, S. A., Ribatet, M. and Sisson, S. A. (2010) Likelihood-Based Inference for
435 Max-Stable Processes. *Journal of the American Statistical Association*, **105**, 263–277.
436 URL`http://www.tandfonline.com/doi/abs/10.1198/jasa.2009.tm08577.`
- 437 Reich, B. J. and Shaby, B. A. (2012) A hierarchical max-stable spatial model
438 for extreme precipitation. *The Annals of Applied Statistics*, **6**, 1430–1451.
439 URL`http://projecteuclid.org/euclid.aoas/1356629046.`
- 440 Thibaud, E., Mutzner, R. and Davison, a. C. (2013) Threshold modeling of extreme spatial rainfall. *Water
441 Resources Research*, **49**, 4633–4644.
- 442 Thibaud, E. and Opitz, T. (2013) Efficient inference and simulation for elliptical Pareto processes. 1–19.
- 443 Wadsworth, J. L. and Tawn, J. a. (2012) Dependence modelling for spatial extremes. *Biometrika*, **99**, 253–
444 272.
- 445 — (2014) Efficient inference for spatial extreme value processes asso-
446 ciated to log-Gaussian random functions. *Biometrika*, **101**, 1–15.
447 URL`http://biomet.oxfordjournals.org/cgi/doi/10.1093/biomet/ast042.`